Photochemically Induced Reversible CO Insertion into Ruthenium-Amido Bonds[1]

Olaf C. P. Beers, Jos G. P. Delis, Wilhelmus P. Mul, Kees Vrieze, and Cornelis J. Elsevier*

Anorganisch Chemisch Laboratorium, Universiteit van Amsterdam, Nieuwe Achtergracht 166, 1018 WV Amsterdam, The Netherlands

Wilberth J. J. Smeets and Anthony L. Spek

Bijvoet Center for Biomolecular Research, Vakgroep Kristal- en Structuurchemie, Universiteit Utrecht, Padualaan 8, 3584 CH Utrecht, The Netherlands

Received October 8, 1992

Upon photolysis of $Ru_2(CO)_6\{MeC{=}C(H)CH_2N\text{-}i\text{-}Pr\}$ (**1**) and $Ru_2(CO)_6\{RCC(H)N\text{-}t\text{-}Bu\}$ (**2a**, R = *i*-Pr; **2b**, R = $PhCH_2$) under an atmosphere of CO, insertion of CO into the Ru-N bond of the amido ligands takes place, affording $Ru_2(CO)_6\{MeC{=}C(H)CH_2N(i\text{-}Pr)C(O)\}$ (**3**) and $Ru_2(CO)_6\{RCC(H)N(t\text{-}Bu)C(O)\}$ (**4a/b**). The X-ray crystal structures of **3** and **4a** have been determined. Crystals of **3** are triclinic, space group $P\bar{1}$, a = 8.733(1) Å, b = 12.841(2) Å, c = 17.261(2) Å, α = 82.79(1)°, β = 77.95(1)°, γ = 72.48(1)°, Z = 4, convergence reached at R = 0.058 for 6028 reflections with $I > 2.5\sigma(I)$. Crystals of **4a** are monoclinic, space group $P2_1/n$, a = 8.222(1) Å, b = 17.877(1) Å, c = 13.592(1) Å, β = 99.34(1)°, Z = 4, convergence reached at R = 0.026 for 3665 observed reflections with $I > 2.5\sigma(I)$. The photolysis of **2a** with PPh_3, yielding the PPh_3-substituted analogue of **4a**, $Ru_2(CO)_5(PPh_3)\{RCC(H)N(t\text{-}Bu)C(O)\}$ (**6a**) revealed that the inserted CO ligand is coordinated to the metal prior to insertion. The same isomer of complex **6a** has also been prepared by initial thermal substitution of CO by PPh_3 in **2a**, yielding $Ru_2(CO)_5PPh_3\{RCC(H)N\text{-}t\text{-}Bu\}$ (**5a**), and its subsequent photochemical reaction with CO.

Introduction

The classic insertion of carbon monoxide into a metal-carbon bond is an important reaction-step in stoichiometric and catalytic organometallic chemistry.[2a] The mechanism of insertion has been studied extensively and it is now generally accepted to occur by the migration of a metal-attached alkyl or aryl group to a cis-coordinated CO ligand.[2]

The insertion of CO into a transition metal-amido bond is less often encountered.[3] A few examples have been reported in the chemistry of the actinides, where the rather strong metal-oxygen interaction, which is usual for this type of metals, probably facilitates the migratory insertion of carbon monoxide into the metal-amido bond.[4] In general, amido complexes of the platinum group metals are not very susceptible to CO insertion. Instead, in reactions with CO, often ligand substitution or addition takes place.[3] An exception has been encountered for $Pt(Ph_2PCH_2CH_2PPh_2)(CH_3)(NHCH_2Ph)$, featuring preferentially insertion of CO into the metal-amido bond. This reaction is particularly interesting, because in the starting complex both a M-C and a M-N bond, in which insertion may take place, are present.

Although CO insertion into metal-amido bonds is rather uncommon, it has been proposed to occur during the conversion of Schiff bases into phtalimidines, which is either catalyzed by cobalt[5,6] or by iron in the stoichiometric reaction between $Fe_2(CO)_9$ and Schiff bases upon oxidation of the resulting amido-type product with $FeCl_3$.[7] Recently, CO insertion into a Co-amido bond was proposed to take place in the $Co_2(CO)_8$-catalyzed carbonylation of azetidines, yielding pyrrolidinones.[8] Another example of CO insertion into a metal-amido bond as part of a complex reaction sequence, has been provided by the 1,3-dipolar cycloaddition reaction of alkynes with metal-heterodiene complexes, whereby 1,5-dihydropyrrol-2-ones are formed stoichiometrically.[9]

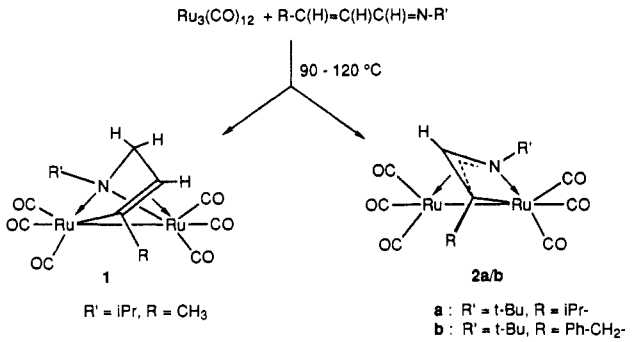

Figure 1. Formation of **1** and **2** by cyclometallation of a monoazadiene on the Ru-carbonyl skeleton.

In our study of the reactivity of monoazadienes $RC(H)_\beta{=}C(H)_\alpha C(H)_{im}{=}NR'$ toward $Ru_3(CO)_{12}$, we have encountered two dinuclear complexes **1** and **2** (Figure 1), which are the first isolable products of the thermal reaction.[10] By replacement of the β-hydrogen atom of the MAD ligand by a Me group, the cyclometalation path leading to the five-membered metallacycle in **1** is blocked. In this case the reaction of $Ru_3(CO)_{12}$ with MAD gives high yields of **2a**.[11] Complexes **1** and **2** possess five- and four-membered azametallacycles, respectively. The bonding

(1) Reactions of Monoazadienes with Metal Carbonyl Complexes. 17. For other parts see refs 10, 11, and 26.
(2) (a) Parshall, G. W. *Homogeneous Catalysis*; Wiley-Interscience: New-York, 1980; Chapter 5. (b) Koga, N.; Morokuma, K. *J. Am. Chem. Soc.* **1986**, *108*, 6136. (c) Calderazzo, F. *Angew. Chem.* **1977**, *89*, 305.
(3) Fryzuk, M. D.; Montgomery, C. D. *Coord. Chem. Rev.* **1989**, *95*, 1.
(4) Fagan, P. J.; Manriquez, J. M.; Vollmer, S. H.; Day, C. S.; Day, V. W.; Marks, T. J. *J. Am. Chem. Soc.* **1981**, *103*, 2206.
(5) Murahashi, S.; Horrie, S. *Bull. Chem. Soc. Jpn.* **1960**, *33*, 247.
(6) Rosenthal, A. In *Organic Synthesis via Metal Carbonyls*; Wender, I., Pino, P., Eds.; Wiley: New York, 1968; Vol 1., p 433.
(7) Bagga, M. M.; Flannigan, W. T.; Kno, G. R.; Pauson, P. L.; Preston, F. J.; Reed, R. I. *J. Chem. Soc. C* **1968**, 36.
(8) Roberto, D.; Alper, H. *J. Am. Chem. Soc.* **1989**, *111*, 7539.
(9) de Lange, P. P. M.; Frühauf, H.-W.; van Wijnkoop, M.; Vrieze, K.; Wang, Y.; Heijdenrijk, D.; Stam, C. H. *Organometallics* **1990**, *9*, 1691.
(10) (a) Mul, W. P.; Elsevier, C. J.; Polm, L. H.; Vrieze, K.; Zoutberg, M. C.; Heijdenrijk, D.; Stam, C. H. *Organometallics* **1991**, *10*, 2247. (b) Elsevier, C. J.; Mul, W. P.; Vrieze, K. *Inorg. Chim. Acta* **1992**, *200*, 689. (c) Polm, L. H.; Elsevier, C. J.; Mul, W. P.; Vrieze, K.; Christophersen, M. J. N.; Muller, F.; Stam, C. H. *Polyhedron* **1988**, *7*, 2521.

0020-1669/93/1332-3640$04.00/0

of the nitrogen atom in these complexes can be best described as that of a bridging amido function (*vide infra*) but alternatively one may invoke the presence of an azaallyl moiety.[10c] Both complexes exhibit fluxionality of the ligand system involving interchange of the π-C=C and σ-C coordination.[10]

In this article we report the photochemically induced CO insertion into the Ru–amido bond of both **1** and **2**. During our investigations in this area, the synthesis of the diiron analogue of **2** and its reaction with CO have been published by Mirkin *et al.*[12,13]

Experimental Section

^{1}H and ^{13}C{^{1}H} NMR spectra were recorded on Bruker AC 100 and AMX 300 spectrometers. The ^{13}C NMR spectra were recorded using an APT pulse sequence. IR spectra were measured on Perkin-Elmer 283 and Nicolet 7199B FTIR (liquid nitrogen cooled, Hg, Cd, Te detector) spectrophotometers using matched NaCl solution cells of 0.5-mm path length. Field desorption (FD) mass spectra were obtained with a Varian MAT711 double focussing mass spectrometer with a combined EI/FI/FD source, fitted with a 10-μm tungsten wire FD-emitter containing carbon microneedles with an average length of 30 μm, using emitter currents of 0–15 mA. Elemental analyses were carried out by Dornis und Kolbe, Mikroanalytisches Laboratorium, Mülheim a.d. Ruhr, Germany. All preparations were carried out under an atmosphere of purified nitrogen. Carefully dried solvents were used. Silica gel for column chromatography (Kieselgel 60, 70-230 mesh, E. Merck, Darmstadt, Germany) was dried before use. Photochemical experiments were performed with a high-pressure mercury lamp in combination with a Pyrex cut-off filter ($\lambda \geq 300$ nm) and water cooling. The complexes $Ru_2(CO)_6$\{MeC=C(H)CH_2N-*i*-Pr\} (**1**)[10] and $Ru_2(CO)_6$\{RCC(H)N-*t*-Bu\} (**2a**, R = *i*-Pr; **2b**, R = $PhCH_2$)[10,11] were prepared according to literature procedures. Reported FD-mass data are based on the highest peak of the isotopic pattern of the molecular ion, which corresponds to ^{102}Ru (calculated value in parentheses).

Synthesis of $Ru_2(CO)_6$\{MeC=C(H)CH_2N(*i*-Pr)C=O\} (3). A solution of $Ru_2(CO)_6$\{MeC=C(H)CH_2N-*i*-Pr\} (**1**; 240 mg, 0.5 mmol) in 50 mL of hexane was irradiated under an atmosphere of CO at 25 °C for 8 h. During this period the color of the solution changed from pale yellow to yellow-orange and a small amount of a red product, which was identified as $[Ru(CO)_4]_n$ by IR spectroscopy,[14] precipitated. The reaction products were separated by column chromatography on silica. With hexane as the eluent 70 mg of unreacted **1** (30%) was obtained. Subsequent elution with hexane/diethyl ether (19:1) afforded 10 mg of $Ru_2(CO)_6$\{MeCC(H)C(H)N=C(Me)$_2$\} (5%).[15] With hexane/diethyl ether (1:1) as the eluent the yellow complex $Ru_2(CO)_6$\{MeC=C(H)CH_2N(*i*-Pr)C=O\} (**3**, 80 mg, 30%) was obtained. Crystals of **3** suitable for X-ray diffraction were obtained from a saturated hexane solution cooled at –30 °C. Anal. Found (calcd) for **3**: C, 33.01 (33.01); H, 2.54 (2.57); N, 2.80 (2.75); FD-mass: *m/e* 510 (*M* = 511).

Synthesis of $Ru_2(CO)_6$\{RCC(H)N(*t*-Bu)C=O\} (4a, R = *i*-Pr; 4b, R = $PhCH_2$). A pale yellow solution of **2a/b** (0.20 mmol) in 50 mL of hexane was irradiated under 1.2 bar of CO. After 8 h the IR spectrum of the resulting light-yellow solution showed quantitative conversion of **2** into **4**. In order to remove traces of impurity the product was chromatographed on silica. Elution with hexane/diethyl ether (19:1) yielded complex **4** in 90–95% yield. Crystals of **4a** suitable for X-ray diffraction were obtained from a saturated hexane solution at –30 °C. Anal. Found (calcd) for **4a**: C, 35.77 (35.76); H, 3.22 (3.16); N, 2.44 (2.61). Found (calcd) for **4b**: C, 40.97 (41.04); H, 2.92 (2.90); N, 2.43 (2.39).

Synthesis of $Ru_2(CO)_5PPh_3$\{*i*-Pr-CC(H)N-*t*-Bu\} (5a). A solution of **2a** (0.10 g, 0.2 mmol) and PPh_3 (0.05 g, 0.2 mmol) in 50 mL of heptane was refluxed for 4 h. The resulting yellow-orange solution was transferred to a silica column. Elution with hexane/dichloromethane (2:1) yielded the yellow complex **5a** (0.10 g, 0.14 mmol, 70%). Anal. Found (calcd): C, 51.55 (51.50); H, 4.25 (4.30); N, 1.93 (1.90). FD-mass: *m/e* 745 (*M* = 745).

Synthesis of $Ru_2(CO)_5PPh_3$\{*i*-PrCC(H)N(*t*-Bu)C=O\} (6a). I. A solution of 0.10 g of **5a** (0.14 mmol) in 40 mL of hexane and just enough THF to obtain a clear solution (about 3 mL) was irradiated under 1.2 bar of CO for 8 h. The resulting solution was chromatographed on silica with CH_2Cl_2 as the eluent, affording the yellow complex **6a** in 0.08 g yield (74%).

II. A solution of 0.10 g of **2a** (0.2 mmol) with 0.05 g of PPh_3 (0.2 mmol) in 50 mL of hexane was irradiated for 4h. After workup (*vide supra*) complex **6a** was isolated in 0.13 g yield (85%). FD-mass: *m/e* 773 (*M* = 773).

Thermal Conversion of Complex 3/4/6 into 1/2/5. A solution of **3**, **4**, or **6** (0.1 mmol) in 20 mL of hexane was stirred at 60 °C for 3 h. During this period quantitative conversion into the complexes **1**, **2**, or **5**, respectively, took place as observed by spectroscopic techniques (IR, ^{1}H NMR). When the same experiment was performed under 1.2 bar of CO, no reaction was observed.

NOE-Difference Experiment for the Complexes 5a and 6a. NMR tubes containing solutions of **5a** and **6a** in $CDCl_3$ were prepared, taking standard precautions for NOE-difference measurements. When the proton resonances of the PPh_3 group in the ^{1}H NMR spectrum of **5a** and **6a** were saturated, in the case of **5a** a NOE was observed at the methine resonance of the *i*-Pr group. For **6a** as well a NOE was observed at the *i*-Pr group but in this case on the Me resonance at 0.89 ppm.

Low-Temperature IR Experiment with Complex 2a. In a low-temperature IR cell, a solution of **2a** in THF (±5 mM) was cooled to –100 °C and the IR spectrum was recorded (*y*-scale: 0–1.4 absorbance). After irradiation for 10 min at –100 °C the IR spectrum was recorded again. The results are depicted in Figure 7. Then the solution was allowed to warm to room temperature and the IR spectrum now showed again the absorptions of the parent complex **2a** with about the same intensities as compared to the starting situation.

Crystal Structure Determination of 3 and 4a. X-ray data were collected on an Enraf-Nonius CAD4 diffractometer (Mo Kα, Zr filtered, λ = 0.710 73 Å). Crystal data are collected in Table I. Both structures were solved with standard Patterson and Fourier techniques (SHELXS86[16]) and refined on *F* by full-matrix least-squares techniques. Neutral atom scattering factors were taken from ref 17 and corrected for anomalous dispersion.[18] All calculations were performed with SHELX76[19] and PLATON[20] (geometrical calculations and illustrations) on a MicroVAX cluster. Positional parameters are listed in Tables II and III.

$Ru_2(CO)_6$\{MeC=C(H)CH_2N(*i*-Pr)C=O\} (3). Data were collected for a brownish rod-shaped crystal mounted on top of a glass fiber. Unit cell parameters were determined from a least-squares treatment of the SET4 setting angles of 25 reflections with $11.3 < \theta < 14.1°$. The unit

Table I. Crystal Data for Complexes **3** and **4a**

	3	4a
chem formula	$C_{14}H_{13}NO_7Ru_2$	$C_{16}H_{17}NO_7Ru_2$
fw	509.4	537.45
a, Å	8.733(1)	8.222(1)
b, Å	12.841(2)	17.877(1)
c, Å	17.261(2)	13.592(1)
α, deg	82.79(1)	90
β, deg	77.95(1)	99.34(1)
γ, deg	72.48(1)	90
V, Å^3	1801.1(4)	1971.3(3)
T, K	295	295
λ, Å	0.710 73	0.710 73
space group	$P\bar{1}$ (No. 2)	$P2_1/n$ (No. 14)
Z	4	4
D_x, g cm^{-3}	1.879	1.811
μ, cm^{-1}	16.8	15.4
R^a	0.0580	0.026
R_w^b	0.0798	0.040

$^a R = \Sigma(|F_o| - |F_d|)/\Sigma|F_o|$. $^b R_w = \{\Sigma w(|F_o| - |F_d|)^2/\Sigma w|F_o|^2\}^{1/2}$.

(11) Mul, W. P.; Elsevier, C. J.; Vuurman, M.; Smeets, W. J. J.; Spek, A. L. To be published.
(12) Mirkin, C. A.; Lu, K.-L.; Geoffroy, G. L.; Rheingold, A. L.; Staley, D. L. *J. Am. Chem. Soc.* **1989**, *111*, 7279.
(13) (a) Mirkin, C. A.; Lu, K.-L.; Snead, T. E.; Young, B. A.; Geoffroy, G. L.; Rheingold, A. L.; Haggerty, B. S. *J. Am. Chem. Soc.* **1991**, *113*, 3800. (b) Mirkin, C. A.; Oyer T. J.; Wrighton, M. S.; Snead, T. E.; Geoffroy, G. L. *J. Am. Chem. Soc.* **1992**, *114*, 1256.
(14) Hastings, W. R.; Baird, M. C. *Inorg. Chem.* **1986**, *25*, 2913.
(15) Mul, W. P.; Elsevier, C. J.; Vrieze, K.; Smeets, W. J. J.; Spek, A. L. *Organometallics* **1992**, *11*, 1891.
(16) Sheldrick, G. M. SHELXS86. Program for crystal structure determination. University of Göttingen, Federal Republic of Germany, 1986.
(17) Cromer, D. T.; Mann, J. B. *Acta Crystallogr.* **1968**, *A24*, 321.
(18) Cromer, D. T.; Liberman, D. *J. Chem. Phys.* **1970**, *53*, 1891.
(19) Sheldrick, G. M. SHELX76. Crystal structure analysis package. University of Cambridge, England, 1976.
(20) Spek, A. L. *Acta Crystallogr.* **1990**, *A46*, C34.

Table II. Final Coordinates and Equivalent Isotropic Thermal Parameters of the Non-Hydrogen Atoms of $Ru_2(CO)_6\{MeC{=}C(H)CH_2N(iPr)C{=}O\}$ (3)

atom	x	y	z	U(eq), Å²
Ru(1)	0.66476(10)	0.76604(6)	0.10317(4)	0.0424(3)
Ru(2)	0.94968(10)	0.68047(6)	0.16042(5)	0.0466(3)
O(1)	0.7237(9)	0.5484(5)	0.2465(4)	0.062(3)
O(2)	0.8313(13)	0.7814(7)	-0.0673(5)	0.092(4)
O(3)	0.3770(11)	0.9584(7)	0.0745(6)	0.098(4)
O(4)	0.5543(15)	0.5672(8)	0.0747(7)	0.127(6)
O(5)	1.2263(13)	0.7476(10)	0.0436(7)	0.124(5)
O(6)	1.1238(11)	0.6025(7)	0.3022(5)	0.081(4)
O(7)	1.0230(14)	0.4663(7)	0.0838(5)	0.114(5)
N(1)	0.6050(9)	0.7386(5)	0.2345(4)	0.039(2)
C(1)	0.8704(16)	0.9369(9)	0.0825(7)	0.075(5)
C(2)	0.7960(12)	0.8554(8)	0.1341(6)	0.051(3)
C(3)	0.8011(13)	0.8415(8)	0.2140(6)	0.056(4)
C(4)	0.6588(13)	0.8153(7)	0.2709(5)	0.048(3)
C(5)	0.4458(12)	0.7216(9)	0.2767(6)	0.058(4)
C(6)	0.3044(12)	0.8123(10)	0.2610(8)	0.078(5)
C(7)	0.4444(15)	0.6974(11)	0.3660(7)	0.084(5)
C(8)	0.7494(11)	0.6361(7)	0.2240(5)	0.043(3)
C(9)	0.7737(16)	0.7759(7)	-0.0025(6)	0.064(4)
C(10)	0.4796(13)	0.8848(9)	0.0860(6)	0.062(4)
C(11)	0.5911(15)	0.6403(9)	0.0862(7)	0.066(4)
C(12)	1.1228(16)	0.7270(12)	0.0876(7)	0.083(5)
C(13)	1.0635(12)	0.6326(9)	0.2473(6)	0.057(4)
C(14)	1.0012(15)	0.5481(11)	0.1096(6)	0.080(5)

[a] U(eq) = one-third the trace of the orthogonalized U.

Table III. Final Coordinates and Equivalent Isotropic Thermal Parameters of the Non-Hydrogen Atoms of $Ru_2(CO)_6\{i\text{-}PrCC(H)N(t\text{-}Bu)C{=}O\}$ (4a)

atom	x	y	z	U(eq), Å²
Ru(1)	-0.25505(3)	0.26485(1)	0.58156(2)	0.0371(1)
Ru(2)	-0.02542(3)	0.15297(1)	0.58271(2)	0.0385(1)
O(1)	0.2767(4)	0.07496(18)	0.6932(3)	0.0846(12)
O(2)	0.0891(4)	0.14975(18)	0.3780(2)	0.0726(10)
O(3)	-0.2519(4)	0.01474(18)	0.5357(3)	0.0900(13)
O(4)	-0.5395(3)	0.15910(19)	0.5188(3)	0.0791(11)
O(5)	-0.2183(4)	0.3006(2)	0.3676(2)	0.0756(13)
O(6)	-0.4927(3)	0.39324(17)	0.6086(3)	0.0755(10)
O(7)	0.2042(3)	0.28479(15)	0.5869(2)	0.0586(9)
N	-0.0233(3)	0.30393(13)	0.66958(17)	0.0362(7)
C(1)	0.0306(4)	0.38346(16)	0.7012(2)	0.0428(9)
C(2)	0.1980(4)	0.3788(2)	0.7684(3)	0.0567(11)
C(3)	0.0398(6)	0.4292(2)	0.6070(3)	0.0662(13)
C(4)	-0.0905(5)	0.4202(2)	0.7604(3)	0.0583(11)
C(5)	0.0853(4)	0.25488(17)	0.6116(2)	0.0411(9)
C(6)	-0.1082(4)	0.25952(17)	0.7310(2)	0.0410(9)
C(7)	-0.1341(4)	0.18465(17)	0.7028(2)	0.0399(9)
C(8)	-0.2242(5)	0.1330(2)	0.7659(3)	0.0551(11)
C(9)	-0.3415(8)	0.1707(3)	0.8241(5)	0.101(2)
C(10)	-0.0979(6)	0.0843(3)	0.8326(4)	0.0860(19)
C(11)	0.1631(5)	0.10224(19)	0.6504(3)	0.0542(11)
C(12)	0.0470(4)	0.15066(19)	0.4529(3)	0.0490(11)
C(13)	-0.1669(5)	0.0649(2)	0.5533(3)	0.0553(11)
C(14)	-0.4346(4)	0.1994(2)	0.5419(3)	0.0527(11)
C(15)	-0.2327(4)	0.2868(2)	0.4462(3)	0.0494(11)
C(16)	-0.4015(4)	0.34639(19)	0.6035(3)	0.0511(11)

[a] U(eq) = one-third of the trace of the orthogonalized U.

cell parameters were checked for the presence of higher lattice symmetry.[21] Reflection profiles were rather broad, the crystal was found to be twinned, and data collection was performed on one of the superimposed twin-lattices. The intensities of 8787 reflections were corrected for *Lp*, for small linear decay (2.9%) of the intensity control reflections during the 50 h of X-ray exposure time, and for absorption (using the DIFABS method,[27] correction range 0.81–1.22) and merged into a unique set of 6041 reflections with $I > 2.5\sigma(I)$. H atoms were introduced on calculated positions (C–H = 0.98 Å) and included in the refinement riding on their carrier atoms with one common isotropic thermal parameter (U = 0.074(7) Å²). All non-hydrogen atoms were refined with anisotropic thermal parameters. Thirteen reflections with $F_o \gg F_c$ were excluded from the final weighted refinement cycles; convergence was reached at R = 0.0580.

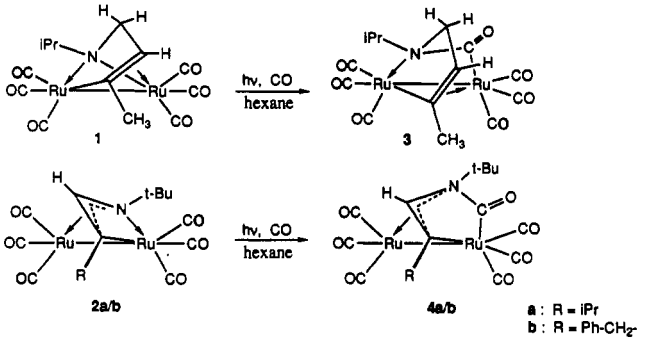

Figure 2. Photochemically induced reactions of **1** and **2** with CO.

$Ru_2(CO)_6\{i\text{-}PrCC(H)N(t\text{-}Bu)C{=}O\}$ (4a). Data were collected for a yellow plate-shaped crystal glued on top of a glass fiber. Unit cell parameters were determined from a least squares treatment of the SET4 setting angles of 25 reflections in the range $14 < \theta < 17°$. The intensities of 4911 reflections were corrected for *Lp* and for absorption (Gaussian integration; correction range 1.21:1.80) and merged into a unique set of 3672 reflections with $I > 2.5\sigma(I)$. H atoms were introduced on calculated positions (C–H = 0.95 Å) and included in the refinement riding on their carrier atoms with two common isotropic thermal parameters. Seven strong low-order reflections were excluded from the final weighted refinement cycles, convergence was reached at R = 0.026.

Results

Formation of the Complexes. Upon irradiation of $Ru_2(CO)_6\{CH_3C{=}C(H)CH_2N\text{-}i\text{-}Pr\}$ (**1**) in hexane solution for 8 h under CO atmosphere, $Ru_2(CO)_6\{MeC{=}C(H)CH_2N(i\text{-}Pr)C{=}O\}$ (**3**) was formed in moderate yields (30%) (Figure 2). Furthermore, small amounts of the byproducts $[Ru(CO)_4]_n$ and $Ru_2(CO)_6\{CH_3CC(H)C(H)N{=}C(Me)_2\}$ were formed, as established by their spectroscopic data. In complex **3** a CO molecule has been inserted into a Ru–N bond, as has been unambiguously established by means of X-ray crystallography (*vide infra*).

In complex **2**,[10c] which contains a four-membered azametallacycle, CO insertion in the Ru–N bond could be effected photochemically as well (Figure 2), but not thermally. The product, $Ru_2(CO)_6[RCC(H)N(t\text{-}Bu)C{=}O\}$ (**4**), was formed almost quantitatively and was analyzed both spectroscopically and by means of an X-ray structure determination (*vide infra*).

In order to obtain more information about the mechanism of the CO-insertion a PPh_3 ligand was introduced in complex **2**, thus creating asymmetry in the metal carbonyl core. Moreover, the ^{31}P-coupling pattern facilitates the elucidation of the molecular structure by NMR spectroscopy. The thermal reaction between **2a** and 1 equiv of PPh_3 resulted in substitution of one CO ligand and $Ru_2(CO)_5PPh_3\{i\text{-}PrCC(H)N\text{-}t\text{-}Bu\}$ (**5a'**) was obtained in good yield (Figure 3). The molecular structure of **5a'** was established by means of spectroscopic techniques (*vide infra*). The photochemical CO insertion reaction was performed with this PPh_3-substituted derivative of **2a** as well. Again, CO insertion into the Ru–N bond occurred, affording complex **6a** (Figure 3). The conversion of **2a** into **6a** could also be effected in one step by irradiation of a solution of **2a** in the presence of 1 equiv of PPh_3 (Figure 3), resulting in the same isomer of **6a** as was obtained via the first route. All insertion products (**3**, **4**, **6**) appeared to be thermally unstable (60 °C in heptane), giving rise to deinsertion of CO and formation of the parent compounds **1**, **2**, and **5**, respectively. The thermal deinsertion reaction at 60 °C could be inhibited by working under an atmosphere of CO.

Molecular Structure of 3. The molecular geometry of **3** along with the adopted numbering scheme is shown in Figure 4 and selected bond lengths and bond angles are given in Table IV. By this X-ray structure determination the position of the inserted CO ligand, *viz.* in the Ru(2)–N bond and not in the Ru(1)–C(2)

(21) Spek, A. L. *J. Appl. Crystallogr.* **1988**, *21*, 578.
(22) Walker, N.; Stuart, D. *Acta Crystallogr.* **1983**, *A39*, 158.

Table IV. Selected Bond Distances (Å) and Angles (deg) for Complex **3** (with Esd's in Parentheses)

Ru(1)–Ru(2)	2.7355(13)	Ru(1)–N	2.225(7)	Ru(1)–C(2)	2.029(11)
Ru(1)–C(9)	1.881(11)	Ru(1)–C(10)	1.905(11)	Ru(1)–C(11)	1.982(2)
Ru(2)–C(2)	2.288(10)	Ru(2)–C(3)	2.276(10)	Ru(2)–C(8)	2.056(10)
Ru(2)–C(12)	1.945(14)	Ru(2)–C(13)	1.907(11)	Ru(2)–C(14)	1.900(13)
O(1)–C(8)	1.215(11)	O(2)–C(9)	1.129(14)	O(3)–C(10)	1.119(15)
O(4)–C(11)	1.131(17)	O(5)–C(12)	1.127(18)	O(6)–C(13)	1.148(14)
O(7)–C(4)	1.140(16)	N–C(4)	1.464(12)	N–C(5)	1.494(14)
N–C(8)	1.523(1)	C(2)–C(3)	1.377(14)	C(3)–C(4)	1.510(15)
N–Ru(1)–C(2)	81.2(3)	C(2)–Ru(2)–C(8)	92.2(4)	C(3)–Ru(2)–C(8)	79.9(4)
C(8)–Ru(2)–C(12)	171.8(5)	C(8)–Ru(2)–C(13)	91.5(4)	C(8)–Ru(2)–C(14)	85.8(5)
Ru(1)–N–C(4)	108.5(5)	Ru(1)–N–C(5)	122.9(6)	Ru(1)–N–C(8)	85.2(4)
C(4)–N–C(5)	114.1(7)	C(4)–N–C(8)	105.8(7)	C(5)–N–C(8)	116.1(7)
Ru(1)–C(2)–Ru(2)	78.4(3)	Ru(1)–C(2)–C(3)	112.3(8)	Ru(2)–C(2)–C(3)	71.9(6)
C(1)–C(2)–C(3)	119.9(10)	Ru(2)–C(3)–C(2)	73.0(6)	Ru(2)–C(3)–C(4)	105.1(6)
C(2)–C(3)–C(4)	118.5(10)	N–C(4)–C(3)	108.1(7)	N–C(5)–C(6)	113.2(9)
N–C(5)–C(7)	111.0(9)	C(6)–C(5)–C(7)	111.3(10)	Ru(2)–C(8)–O(1)	133.4(7)
Ru(2)–C(8)–N	108.4(5)	O(1)–C(8)–N	117.8(9)		

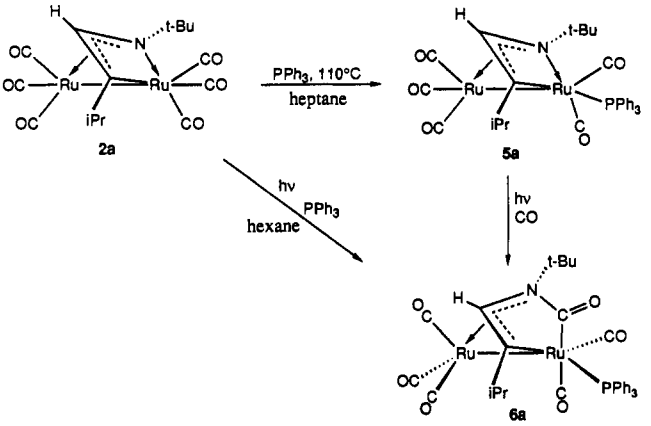

Figure 3. Two reaction routes for the preparation of **6a**.

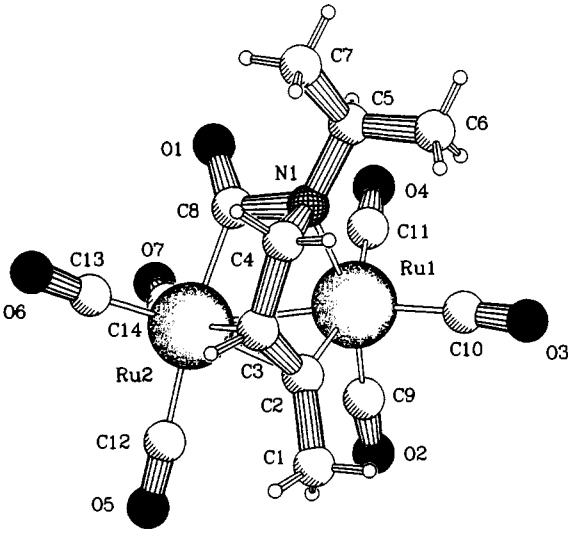

Figure 4. Molecular structure of $Ru_2(CO)_6\{MeC{=}C(H)CH_2N(i\text{-}Pr)C(O)\}$ (**3**). Only one of the two nearly identical molecules is shown.

bond, has been indisputably ascertained. Of the two crystallographically independent molecules in the unit cell, only one will be discussed.[23] The intermetallic distance has slightly increased from 2.666(2) Å in **1**[10a] to 2.7355(13) Å in **3**, which values are indicative of a normal single Ru–Ru bond.[24] The 5-membered metallacycle, which is also present in **1**, is unaffected in **3**. The influence of the inserted CO ligand has been most profoundly

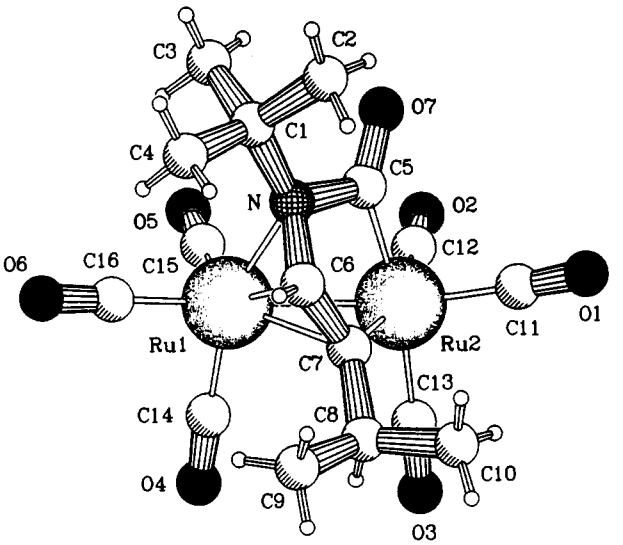

Figure 5. Molecular structure of $Ru_2(CO)_6\{i\text{-}PrCC(H)N(t\text{-}Bu)C(O)\}$ (**4a**).

expressed by a significant elongation of the Ru(1)–N bond (**3**, 2.225(7) Å, vs. **1**, 2.136(3) Å), whereas the Ru(1)–C(2) bond in **3** (2.029(11) Å) is slightly shorter than that in **1** (2.066(4) Å). The CO ligand which has been inserted into the Ru–N bond is bonded in the usual fashion. For example the length of the Ru(2)–C(8) bond (2.056(10) Å) compares to the length of the Ru–C bond (2.078(8) Å) in $Ru(CO)_3I\{C(O)Me\}$ {*i*-Pr-DAB},[25] which contains a CO ligand inserted into a Ru–C bond. The value of 1.523(11) Å for the C(8)–N bond length falls in the range of 1.48–1.53 Å, which is generally observed for C–N single bonds. This implies that the C(8)–N bond has a bond order of 1; hence, no conjugation effects are involved.

Molecular Structure of 4a. The molecular geometry of **4a** is shown in Figure 5 and selected bond distances and angles are given in Table V. This X-ray structure determination unambiguously confirms the insertion of a carbonyl ligand into the Ru–N bond of the metallacycle, which contrasts to the structure of **3**, where insertion of CO has taken place into the exometallacyclic Ru–N bond. The structural data of **4a** can best be compared with the corresponding data of complex **2**[10c] and the isostructural diiron analogues of **2** and **4**, which have been reported recently.[13a] The organic ligand (*i*-Pr)CC(H)N(*t*-Bu)C=O, which bridges the formal single Ru–Ru bond (2.7487(5) Å[24]), is η^3-azaallylic bonded to Ru(1) via C(6), C(7), and N and is coordinated to Ru(2) via σ-bonds of C(5) and C(7). The carbon

(23) The data of the second nearly identical molecule can be found in the supplementary material.

(24) Bennett, M. A.; Bruce, M. I.; Matheson, T. W. In *Comprehensive Organometallic Chemistry*, Wilkinson, G., Stone, F. G. A., Abel, E. W., Eds.; Pergamon Press: Oxford, England, 1982; Vol. 4, p 691.

(25) (a) Kraakman, M. J. A.; de Klerk-Engels, B.; de Lange, P. P. M.; Vrieze, K.; Smeets, W. J. J.; Spek, A. L. *Organometallics* **1992**, *11*, 3774. (b) Chihara, T.; Aoki, K.; Yamazaki, H. *J. Organomet. Chem.* **1990**, *383*, 367.

Table V. Selected Bond Distances (Å) and Angles (deg) for Complex **4a** (with Esd's in Parentheses)

Ru(1)–Ru(2)	2.7487(5)	Ru(1)–N	2.193(2)	Ru(1)–C(6)	2.190(3)
Ru(1)–C(7)	2.287(3)	Ru(1)–C(14)	1.892(4)	Ru(1)–C(15)	1.919(4)
Ru(1)–C(16)	1.944(3)	Ru(2)–C(5)	2.046(3)	Ru(2)–C(7)	2.063(3)
Ru(2)–C(11)	1.900(4)	Ru(2)–C(12)	1.952(4)	Ru(2)–C(13)	1.960(4)
C(11)–O(1)	1.128(5)	C(12)–O(2)	1.127(5)	C(13)–O(3)	1.138(5)
C(14)–O(4)	1.129(5)	C(15)–O(5)	1.121(5)	C(16)–O(6)	1.134(4)
C(5)–O(7)	1.209(4)	N–C(1)	1.530(4)	N–C(5)	1.554(4)
N–C(6)	1.416(4)	C(6)–C(7)	1.399(4)	C(7)–C(8)	1.531(5)
N–Ru(1)–C(6)	37.68(10)	N–Ru(1)–C(7)	64.46(10)	C(6)–Ru(1)–C(7)	36.34(1)
Ru(1)–Ru(2)–C(5)	68.71(9)	Ru(1)–Ru(2)–C(7)	54.51(8)	C(5)–Ru(2)–C(7)	80.80(12)
Ru(1)–N–C(1)	129.47(18)	Ru(1)–N–C(5)	93.64(16)	Ru(1)–N–C(6)	71.04(16)
C(1)–N–C(5)	120.20(20)	C(1)–N–C(6)	120.20(20)	C(5)–N–C(6)	111.20(20)
Ru(2)–C(5)–O(7)	134.10(20)	Ru(2)–C(5)–N	108.99(19)	O(7)–C(5)–N	116.60(30)
Ru(1)–C(6)–N	71.28(15)	Ru(1)–C(6)–C(7)	75.58(17)	N–C(6)–C(7)	116.30(30)
Ru(1)–C(7)–Ru(2)	78.20(9)	Ru(1)–C(7)–C(6)	68.08(16)	Ru(1)–C(7)–C(8)	126.10(20)
Ru(2)–C(7)–C(6)	114.40(20)	Ru(2)–C(7)–C(8)	126.10(20)	C(6)–C(7)–C(8)	119.30(30)

Table VI. IR and ^{31}P NMR Data[a] for $Ru_2(CO)_6\{CH_3C{=}C(H)CH_2N(i\text{-}Pr)CO\}$ (**3**), $Ru_2(CO)_6\{RCC(H)N(t\text{-}Bu)CO\}$ (**4**), $Ru_2(CO)_5(PPh_3)\{RCC(H)N\text{-}t\text{-}Bu\}$ (**5**), $Ru_2(CO)_5(PPh_3)\{RCC(H)N(t\text{-}Bu)CO\}$ (**6**) [**a**, R = *i*-Pr; *b*, R = $PhCH_2$]

	ν(CO), cm^{-1}					$\nu(CO)_{ins}$	^{31}P NMR, ppm
3	2087 (m)	2057 (vs)	2018 (s)	2012 (s)	1990 (m)	1682 (w)	
4a	2083 (m)	2048 (s)	2018 (s)	2001 (m)	1988 (m)	1727 (w)	
4b	2083 (m)	2049 (s)	2020 (s)	2004 (m)	1996 (w)	1726 (w)	
					1989 (m)		
5a	2051 (vs)	1996 (s)	1995 (sh)	1987 (s)	1980 (s)		37.8
		1973 (m)	1965 (s)	1948 (w)	1934 (w)		
6a	2059 (s)	2001 (vs)	1980 (m)	1961 (w)		1702 (w)	47.9

[a] IR data for hexane solutions; ^{31}P-NMR data in $CDCl_3$, at 120 MHz, 293 K, shifts are relative to 85% H_3PO_4 as external standard, positive shifts to higher frequency.

Table VII. ^1H NMR Data[a] for $Ru_2(CO)_6\{CH_3C{=}C(H)CH_2N(i\text{-}Pr)CO\}$ (**3**), $Ru_2(CO)_6\{R\text{-}CC(H)N(t\text{-}Bu)CO\}$ (**4**), $Ru_2(CO)_5(PPh_3)\{RCC(H)N\text{-}t\text{-}Bu\}$ (**5**), $Ru_2(CO)_5(PPh_3)\{RCC(H)N(t\text{-}Bu)CO\}$ (**6**) [**a**, R = *i*-Pr; **b**, R = $PhCH_2$]

	$H_{im/am}$	R/CH_3	N-*t*-Bu/N-*i*-Pr	PPh_3
3[b]	2.14 (dd, 11, 1.5)	2.47 (s) 4.29 (br s)[c]	3.38 (sept, 6.5)	
	1.89 (d, 11)		0.67/0.64 (d, 6.5)	
4a[d]	6.76 (s)	2.94 (sept, 7.0), 1.36/1.23 (d, 7.0)	1.39 (s)	
4b[e]	6.74 (s)	4.00 (s), 7.41–7.27 (m)	1.39 (s)	
5a[e]	6.33 (d, 3.8)	1.92 (sept, 6.8), 0.85/0.84 (d, 6.8)	0.79 (s)	7.57–7.26 (m)
6a[d]	6.88 (s)	2.85 (sept, 6.8), 1.11/0.89 (d, 6.8)	1.35 (s)	7.50–7.33 (m)

[a] Suffixes to atoms refer to $R(CH)_\alpha(CH)_{im/am}NR'$ and conform to the numbering in the monoazadiene ligand system from which the compounds are derived. [b] 100.13 MHz, C_6D_6, 293 K. [c] H_α. [d] 100.13 MHz, $CDCl_3$, 293 K. [e] 300.13 MHz, $CDCl_3$, 293 K.

Table VIII. ^{13}C NMR Data[a] for $Ru_2(CO)_6\{CH_3C{=}C(H)CH_2N(i\text{-}Pr)CO\}$ (**3**), $Ru_2(CO)_6\{RCC(H)N(t\text{-}Bu)CO\}$ (**4**), $Ru_2(CO)_5(PPh_3)\{RCC(H)N\text{-}t\text{-}Bu\}$ (**5**), $Ru_2(CO)_5(PPh_3)\{RCC(H)N(t\text{-}Bu)CO\}$ (**6**) [**a**, R = *i*-Pr; **b**, R = $PhCH_2$]

	$C_{im/am}$	C_α	R/CH_3–C	N–R′	Ru–CO	$(CO)_i$	PPh_3
3[b]	51.3	79.3	191.9, 37.3	50.3, 21.7/18.4	198.6, 198.5, 197.6, 195.1, 194.1, 193.6	207.2	
4a[b]	99.6	179.8	44.3, 30.6/25.7	61.1, 31.5	200.5, 199.6, 197.6 (3C), 195.4	206.8	
4b[c]	100.6	167.8	59.2, 141.1, 129.2, 127.3	50.6, 29.6	198.9, 198.0, 195.8 (3C), 192.6	205.0	
5a[d]	111.4 (d,2)	144.5	34.2, 26.2/24.6	55.4, 30.1	206.0 (d, 10), 204.7 (d, 8), 198.5 (3C)		136.8 (d, 39), 133.1 (d, 12) 129.6 (d, 2), 128.1 (d, 10)
6a[e]	96.9	181.9	41.9, 24.4/22.7	57.9, 29.4	204.5 (d, 7.5), 202.8 (d, 9), 196.5 (3C)	211.8 (d, 10)	136.9 (d, 43), 133.4 (d, 12), 129.7 (d, 1), 128.0 (d, 10)

[a] Suffixes to atoms refer to $R(CH)_\alpha(CH)_{im/am}NR'$ and conform to the numbering in the monoazadiene ligand system from which the compounds are derived. $(CO)_i$ is the abbreviation for inserted CO. [b] 25.1 MHz, $CDCl_3$, 263 K. [c] 75.46 MHz, $CDCl_3$, 243 K. [d] 75.46 MHz, $CDCl_3$, 293 K. [e] 75.46 MHz, $CDCl_3$, 263 K.

atom C(7) is 0.22 Å closer to Ru(2) than to Ru(1), consistent with it being σ-bonded to Ru(2) and π-bonded to Ru(1).

The intraligand distances in the azaallylic moiety, C(6)–C(7) (1.399(4) Å), and C(6)–N (1.416(4) Å), compare very well to the corresponding values in the Fe_2 analogue of **4** (1.394(21) and 1.423(8) Å, respectively[13a]). The N–C(5) distance of 1.554(4) Å is longer than normally observed for single C–N bonds (1.48–1.53 Å). In the diiron analogue of **4** the corresponding C–N distance of 1.605(19) Å is even longer. These elongated C–N bonds may point to a rather weak bonding between the organic ligand and the inserted carbonyl. The carbonyl carbon C(5) lies 0.19(1) Å out of the least-squares plane defined by the five atoms of the metallacycle, illustrating that the 5-membered metallacycle deviates significantly from planarity.

Spectroscopic Analysis of the Complexes 3–6. The spectroscopic data for the new complexes **3–6** are given in Tables VI–VIII.

Compound 3. Upon CO insertion the coordination mode of the organic ligand in **3** has only been slightly influenced, which is reflected by the NMR chemical shifts. Most characteristic are the chemical shift values for H_α/C_α (**3**, 4.29/79.3 ppm, vs. **1**, 4.96/77.9 ppm[10]) and for H_{im}/C_{im} (**3**, 2.14 + 1.89/51.3 ppm, vs. **1**: 3.77/63.4 ppm[10]). The dynamic process as observed in the NMR spectra of the parent compound **1** at 293 K, can no longer take place, due to the inserted CO ligand. Therefore, the ^1H NMR spectrum of **3** resembles the spectrum of **1** recorded at 263 K, where the fluxional process was frozen on the NMR time scale.[10] Consequently, the H atoms of the CH_2 moiety (H_{am}) in

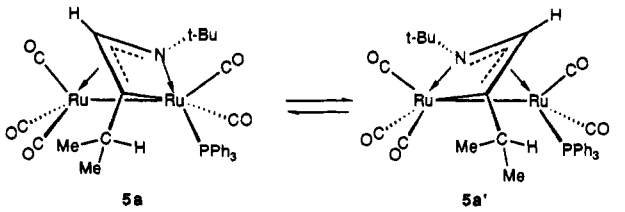

Figure 6. Schematic drawing of the proposed molecular structure of **5a** and its dynamic behavior in solution.

3 are magnetically inequivalent and appear as doublets (J_{gem} = 11 Hz). Only one of the methylene hydrogen atoms shows ^3J coupling to H_α (1.5 Hz). The ^{13}C resonance of the inserted carbonyl is found at 207.2 ppm, which is a normal value for an organic carbonyl group.

Compounds 4–6. Complexes **4–6** all possess an η^3-azaallylic coordinated organic ligand. The H_{im}/C_{im} resonances are found in the range 6.3–6.9/9.7–111 ppm respectively, which values compare well with the corresponding figures for **2** (6.7–6.9/108–110 ppm).[10] The resonances of the metalated carbon atom C_α, however, differ by about 30–35 ppm between the complexes **2a/2b/5a** (147.2, 140.9, and 144.5 ppm, respectively) and their CO-inserted counterparts **4a/4b/6a** (179.8, 167.8, and 181.9 ppm, respectively). The chemical shift value for C_α of about 180 ppm as found in **4a/4b/6a** corresponds well to the value of 180–190 ppm found for the metalated carbon atom in other π-coordinated 5-membered azaruthenacycles, like in **1** and **3** or as in previously reported $Ru_{2/3/4}$– or FeRu–monoazadienyl complexes.[10,11,15,26] Compared to these, the resonance of C_α in **2** and **5** is observed at a rather low frequency. The reason for this anomalous shift is not completely clear, but it might be caused by ring strain in the four-membered metallacycle, which is relieved upon CO insertion.

The structures of the complexes **5a** and **6a** can be assigned on the basis of their spectroscopic data (Table IV–VI) and by NOE-difference experiments. The IR spectrum of **5a** shows nine absorption bands in the CO stretching region, from which the presence of two isomers can be deduced. The ^1H, ^{13}C, and ^{31}P NMR spectra of **5a**, however, each show only one set of resonances, even when recorded at 213 K. Hence, complex **5a** is likely to be involved in a dynamic process, probably oscillation of C_{im} between the two Ru centers, as was described previously for **2**.[10] Apparently, this process is fast on the NMR time-scale, but frozen on the relatively fast IR time scale.

Rapid CO scrambling takes place in the $Ru(CO)_3$ unit of **5a** at 293 K, as can be seen from the single resonance at 198.5 ppm in the ^{13}C NMR spectrum. In ^{13}C NMR two doublets ($^2J(P,C)$ = 8–10 Hz) are observed for the CO ligands of the $Ru(CO)_2PPh_3$ moiety, which is indicative for a *cis*-geometry of each CO relative to the PPh_3 ligand. A small $J(P,H)$ and $J(P,C)$ is also found for the resonances of H_{im} (3.8 Hz) and C_{im} (2 Hz), respectively. Because no coupling with ^{31}P is observed on the C_α-resonance, the ^{31}P nucleus probably couples to H_{im}/C_{im} via the N-atom. The structure of **5a**, as is proposed in Figure 6 is in agreement with the observed coupling pattern. Due to the rapid interconversion of **5a** and **5a'** in solution at 293 K, the $J(P,H)$ and $J(P,C)$ to H_{im} to C_{im}, respectively, will be averaged. A NOE-difference spectrum of **5a/5a'**, which shows enhancement at the *i*-Pr methine proton upon irradiation at the PPh_3 proton resonances implying spatial proximity of both parts of the molecule, corroborates the molecular geometry as depicted in Figure 6.

Compound **6a** could be prepared via two different routes (*vide supra*). In both cases the products exhibit the same spectroscopic features, which are assigned to the isomer of **6a** shown in Figure 3. In contrast to **5**, complex **6a** contains a static ligand system

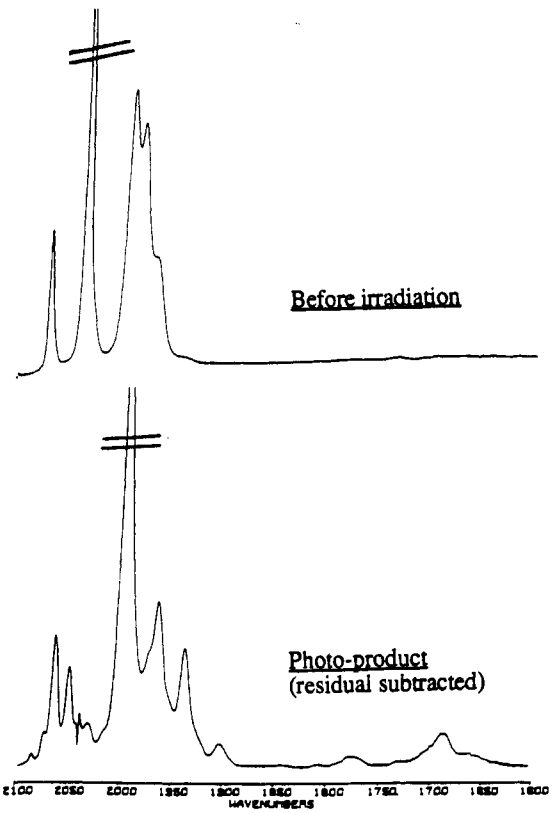

Figure 7. IR spectra recorded upon photolysis of **2a** in THF at 183 K.

on the NMR time scale, because the IR spectrum shows only four absorption bands in the region 2100–1900 cm^{-1}. The IR absorption of the inserted carbonyl in **6a** has shifted by about 25 cm^{-1} to lower energy as compared to the unsubstituted complex **4a**. Such an effect should only be expected if the PPh_3 group and the organic carbonyl are attached to the same Ru atom.

In **6a** a measurable $J(P,C)$ is present only on the ^{13}C resonance of the inserted carbonyl ligand. The magnitude of the coupling constant (10 Hz) points to a cis arrangement of the PPh_3 ligand and the inserted CO ligand.[27] Again the NOE-difference spectrum has revealed spatial proximity of the PPh_3 ligand and the *i*-Pr group. These data completely define the molecular geometry of **6a** as the one depicted in Figure 3.

Discussion

At first sight the organic ligands in complex **1** and **2** seem rather different, but in fact they are quite similar. In **1** the amido nitrogen bridge is attached to the C=C unit via a bridging methylene moiety, whereas in **2** this situation differs only by the absence of the methylene bridge. Now the amido lone pair is in conjugation with the C=C bond, forming together a formally four-electron-donating monoanionic azaallyl moiety, which is π-coordinated to one Ru atom. The other Ru atom is part of the metallacycle and is bonded by the ligand via the metallated carbon atom and the lone pair on the N atom.[28]

There are also appears to be similarity in the fluxional behavior of the organic ligand in each compound. The dynamic processes in both **1** and **2** can be described as an interchange of the π-C=C and σ-C bonds.[10] The methylene-bridge hampers the "windshield-wiper" type oscillation, as in **1** this process can already be frozen on the NMR time scale at 263 K, while **2a** is still fluxional at 193 K.

(26) Beers, O. C. P.; Elsevier, C. J.; Smeets, W. J. J.; Spek, A. L. *Organometallics*, in press.

(27) Xue, Z.; Sieber, W. J.; Knobler, C. B.; Kaesz, H. D. *J. Am. Chem. Soc.* **1990**, *112*, 1825.

(28) The bonding via the formal charge–lone pair of the amido function has been indicated in a Lewis structure by a normal line, while the donative interaction of the normal lone pair on the N-atom has been drawn with an arrow (see Scheme I).

Scheme I. Visualization of the Analogy between the Insertion of CO in **1** and **2**[a]

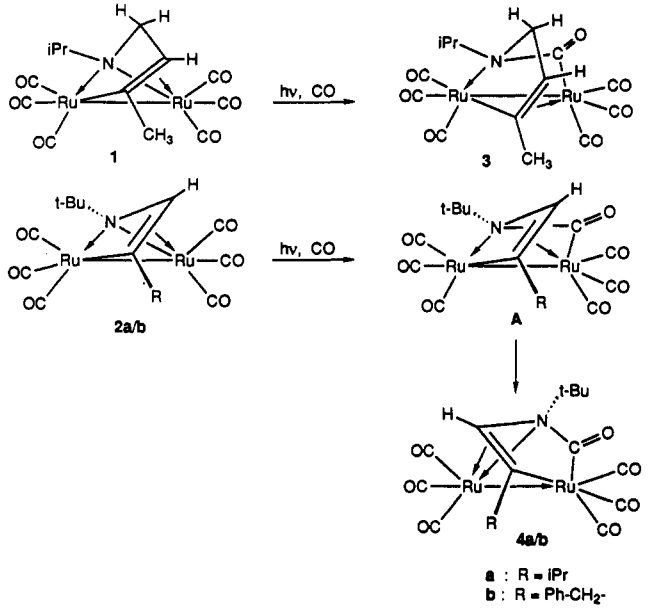

[a] Bonding of the formal charge lone pair of the amido function is indicated by a line, while the donative bond via the lone pair on N is indicated by an arrow.

As a consequence of the bonding description in **1** and **2**, affording Ru atoms in the same oxidation state in both complexes (viz. Ru(1)), the photochemical reaction of **1** with CO involves insertion of a carbonyl ligand into the formal Ru–amido bond,[29] leaving the five-membered metallacycle unaltered in product **3**. When the reaction of **2** with CO would also involve the formal Ru–amido bond by analogy with the reaction of **1** with CO, then complex A (Scheme I) would be expected as the initial insertion product. The formal oxidation state of the metal atoms in both **3** and A has not changed upon CO insertion. Complex A has not been isolated, but instead the isomeric complex **4** has been obtained, featuring the inserted carbonyl as part of the metallacycle. Hence an isomerization, involving a flip of the π-C=C coordination, induces a change of the formal oxidation states, going from two Ru(I) atoms in A to one Ru(0) atom and a Ru(II) atom in **4**, while concomitantly the intermetallic bond becomes a donative one. The driving force for this rearrangement might well be the reduction of the ring-strain in the four-membered metallacycle in A upon isomerization to **4**.

In the PPh_3-containing analogue of **2**, i.e. complex **5**, the ligand system performs an oscillation process like that in **2**, which hampers the intended distinction between both metal atoms. Nevertheless, the experiment with PPh_3 does reveal some mechanistic details.

The first aspect concerns the direct route for the preparation of **6a** and **2a** by irradiation of a solution of **2a** in the presence of PPh_3. This experiment shows, that first a coordinated CO ligand inserts into the Ru–N bond, whereafter an additional ligand (PPh_3) occupies the open coordination site on the metal core. A second point is the finding that the same isomer of **6a** has been obtained via two different routes. Especially the photochemical reaction of **5a** with CO exhibits remarkable selectivity (see Scheme II). Assuming the mechanism in Scheme I to be correct, complex **6a** is formed selectively from complex **5a'** (Scheme II), which is in rapid equilibrium with **5a** as pointed out above. Insertion of CO in the Ru–amido bond of **5a** would lead to an isomeric form of **6a**, complex **6a'**. It may be that CO inserts in both **5a** and **5a'**, but the deinsertion from **6a'** is very fast and drives the equilibrium

Scheme II. Schematic Representation of the Selective Formation of **6a** from **5a** and CO in the Presence of Light

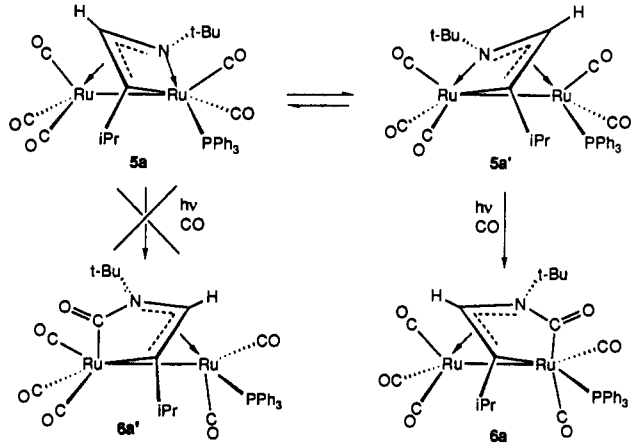

toward **6a**. On the other hand, the selectivity of the reaction can be rationalized by the preferred insertion of CO into the N–Ru-$(CO)_2PPh_3$ bond. An explanation for this phenomenon might be the weakened bonding of the bridging amido-atom towards the $Ru(CO)_2PPh_3$ moiety as compared to the $Ru(CO)_3$ unit, due to the trans-influence of the PPh_3 group. The PPh_3 group of course also induces an increase of π-back-bonding to the CO ligands with concomitant reduction of the electrophilic character of the carbonyl C atom,[29] resulting in a less favourable nucleophilic attack of the amido atom on one of the cis-coordinated carbonyl ligands.

The role of these CO insertion reactions appeared to be crucial. Thermally, no insertion could be effected, which is in contrast to the diiron–analogue of **2**, for which thermally induced (22 °C) insertion of CO into the Fe–C bond has been observed.[13a] In the case of **4** and **6**, deinsertion of CO was effected thermally and **2** and **5**, respectively, were formed.

In the present compounds there are three relevant possibilities for activation of the molecule by light. The first one concerns the activation of the Ru–Ru bond, leading to a biradical species. Such a type of activation has also been proposed for photochemical reactions of $Ru_3(CO)_{12}$,[30] but in the present case the breaking of the intermetallic bond is difficult to associate with CO insertion. A second type of activation is the weakening of the Ru–N bond, which would make the nitrogen atom more nucleophilic and might facilitate the nucleophilic attack of the nitrogen atom on a coordinated CO ligand. This type of activation has been proposed very recently in the case of the diiron analogue of **2** on the basis of the IR shifts of the carbonyl vibrations of the initial photoproduct as compared to the starting complex.[13b] Photochemical breaking of the metal–N bond could also be the operating process in the case of the Ru_2 complexes, but a third type of activation, involving the photochemically induced breaking of the π-C=C coordination, should not be ruled out. The latter type of photochemical activation has been observed or proposed for other monoazadiene(yl) complexes. Matrix photolysis of Fe-$(CO)_3(\eta^4$-Ph-C(H)=C(H)C(H)=NR) has been reported to cause breaking of the π-C=C coordination.[31] Also in the linear chain complex $Ru_4(CO)_{10}\{CH_3C{=}C(H)C(H){=}N\text{-}i\text{-}Pr\}_2$ the π-C=C coordination was proposed to be broken selectively by light, giving rise to C–H activation of the *i*-Pr group on the N atom,[15] and in the photochemical reaction of **1** with $Fe_2(CO)_9$, breaking of the π-C=C coordination induced by light was proposed to be the first step in the formation of FeRu complexes.[26]

(29) Darensbourg, M. Y.; Ash, C. E.; Arndt, L. W.; Janzen, C. P.; Youngdahl, K. A.; Park, Y. K. *J. Organomet. Chem.* **1990**, *383*, 191.

(30) (a) Brodie, N. M. J.; Huq, R.; Malito, J.; Markiewicz, S.; Poë, A. J.; Sekhar, V. C. *J. Chem. Soc., Dalton Trans.* **1989**, 1933. (b) Ford, P. C. *J. Organomet. Chem.* **1990**, *383*, 339.

(31) Kokkes, M. W.; Beentjes, P. C. J.; Stufkens, D. J.; Oskam, A. *J. Organomet. Chem.* **1986**, *306*, 77.

The exact mechanism of the photochemically induced CO insertion remains unclear.

The photochemical reaction of **2** as compared to that of **1** is much more efficient. In the case of **1** the yield of the deinsertion product **3** is only moderate (30%) and two byproducts, $[Ru(CO)_4]_n$ and $Ru_2(CO)_6\{CH_3CC(H)C(H)N{=}C(CH_3)_2\}$, have been formed. Their formation can be explained by the photochemically induced breaking of the π-C=C coordination and by subsequent activation of one of the C–H bonds of the methylene group. The resulting hydrido complex then dimerizes to the tetranuclear complex $Ru_4(CO)_{10}\{CH_3C{=}C(H)C(H){=}N\text{-}i\text{-}Pr\}_2$, which is known to produce $Ru_2(CO)_6\{CH_3CC(H)C(H)N{=}C(CH_3)_2\}$ and ruthenium carbonyl in a photochemical reaction with CO.[15] This C–H activation reaction can not occur in the case of **2**, which explains the much more efficient CO-insertion reaction of the latter. Finally, the reduction of the ring strain in the four-membered azametallacycle in **2** upon CO insertion may also be an important factor determining the efficency of the reaction.

Acknowledgment. The crystallographic part of this work was supported by the Netherlands Foundation for Chemical Research (SON) with financial aid from the Netherlands Organization for Scientific Research (NWO). Thanks are due to A. J. M. Duisenberg for the X-ray data collection and to G. C. Schoemaker for performing the IR measurements at low temperature.

Supplementary Material Available: Thermal motion ellipsoids plots and tables of crystal data, fractional coordinates and isotropic thermal parameters of the hydrogen atoms, anisotropic thermal parameters of the non-hydrogen atoms, and all bond distances and angles for **3** and for **4a** (14 pages). Ordering information is given on any current masthead page.